International Journal of Signal Processing, Image Processing and Pattern Recognition
Vol. 8, No. 1 (2015), pp. 33-48
http://dx.doi.org/10.14257/ijsip.2015.8.1.04

Lake Surface Area Estimation Method based on Error Mechanism Model for Satellite Imagery and Its Application in Ebinur Lake

Rong Xu, Chunzhe Zhao and Jiang Xiong

School of Computer Science and Engineering, Chongqing Three Gorges University, Chongqing 404000, China
xurong010504@163.com

Abstract

A novel mechanism model is proposed for the difference between the lake water areas derived from the remote sensing images at high spatial resolution and low spatial resolution. The areas estimated by images at different spatial resolution are calculated theoretically for the elliptical (including circular), triangular and hexagonal areal ground features. Based on the ideal cases, the quantitative rule between the two kinds of area is summarized. According to the theoretical results, the mechanism model is established for the error of the lake surface area. Especially, the surface area of Ebinur Lake derived with SPOT/VEGETATION (VGT), Landsat EM/ETM+ and MODIS are employed to validate the effectiveness and applicability of this model. With the help of the linear regression method, this model can be used to estimate the error between the Ebinur Lake surface areas derived from satellite images at different spatial resolutions, and promote the lake surface area from low spatial resolution imagery. Consequently, this model is helpful for estimating the lake surface area more accurately in a large region, and its effectiveness can be improved with more historical data.

Keywords: *Error Model, Spatial Resolution, Ebinur Lake, Area Calibration, Remote Sensing*

1. Introduction

Lakes act as the essential components of the hydrological cycle and local ecosystems. Lake area changes are highly sensitive to both climate change and human activities [1]. Therefore, mapping lakes and detecting their area changes accurately and rapidly are of great significance to understand the relevance of lake variations to climate changes and human activities, and they are also crucial to developing, utilizing and protecting of lake water resources [2].

Remote sensing technology is the most efficient and often used method to study changes in lake water area, as it provides synoptic and repeated information. According to the spatial resolution, remote sensing images can be roughly divided into two categories: the high resolution images such as Landsat TM/ETM+, ASTER and SPOT [3-5]; and the low resolution images such as MODIS and NOAA/AVHRR [6-9]. The high resolution images can obtain the lake information accurately, but their temporal resolution is relatively low. For lakes experiencing rapid and significant short-term fluctuations, these low frequency measurements may not adequate to capture these changes [7]. In addition, it is difficult to establish a long-term observation of a region using high resolution imagery [9]. The low resolution images have an advantage of monitoring large-scale lakes with high frequency, and are commonly used to study the long-term trend of lake area. However, due to the low spatial resolution, the accuracy of the area derived from these images is relatively low. In addition to lakes, other land cover types are also facing similar

ISSN: 2005-4254 IJSIP

problems: low resolution satellite data can provide abundant macroscopic information but it is difficult to ensure detailed information of certain precision at the same time [10].

To enable remote sensing monitoring has both high temporal resolution and area estimation accuracy, there are already some studies, which can be broadly divided into two categories: (1) using the mixed pixel decomposition to improve the area accuracy estimated from low resolution imagery; and (2) calibrating the low spatial resolution imagery with the high spatial resolution remote sensing imagery. The mixed pixel decomposition is used to decompose the mixed pixels as several components or end member so as to improve classification accuracy of remote sensing images [11]. For example, Zhang et al. used the multi-endmember linear spectral unmixing technique to estimate the lake fraction in each mixed pixel of MODIS imagery, and develop an algorithm to locate spatially the water body within mixed pixels [9]. To improve the accuracy and applicability of decomposition of mixed pixels, a model combing double-edge extraction with decomposition of mixed pixels was proposed, and attested by computing lake areas of northwestern China using AVHRR imagery [2]. More recently, Liu et al. improved linear mixture model and applied it to extract water body based on MODIS reflectance images, and it indicated that the final result has a high accuracy with the impact of shade corrected [8]. Unlike the mixed pixel decomposition, the second method can comprehensive the advantages of different remote sensing images. Therefore, it improves the estimation accuracy as well as the temporal resolution. For example, Landsat TM imagery was used to improve the rice area estimated from NOAA/AVHRR based on the linear statistical model, the parameter of which is the ratio of the estimated area from NOAA/AVHRR and that from Landsat TM [12]. Gao et al. made a similar study in 2008, and the results show that the method is highly applicable to monitoring variation of the acreage of paddy fields within medium- and small-spatial scale [13]. In addition, a correction model using Landsat TM data to improve the area extracted from NOAA AVHRR was constructed [10]. Recently, to estimate the shelter forest area in Three-North Shelter Forest Program region in 1978-2008, the calibration formulae for the shelter forest area in different precipitation climate regions estimated by the SPOT5 (2.5 m in resolution) and Landsat TM (30 m in resolution) were constructed[14]. In these studies, the linear statistical model was used to calibrate low spatial resolution images with relatively high spatial resolution images besides of constructing the calibration formulae, there are other approaches. For example, a novel spatial-temporal SRM based on a Markov random field is proposed using a current coarse spatial resolution MODIS image and a previous medium spatial resolution Landsat TM image as input, and the results show that this model can generate forest maps with higher overall accuracy and kappa value[15]. A data fusion method for land cover classification is proposed that combines remote sensing data at a fine and a coarse spatial resolution [16]. Although the approaches used in the above studies are not completely the same, they can improve the area accuracy at low expense. However, reasons for difference between the areas from different spatial resolution images were rarely analyzed. When lack sufficient high spatial resolution images to cover the entire study area or the monitoring period, this method can also be used.

Previous studies showed that the lake surface area values derived from different spatial resolution images are strongly correlated [17]. However, there are very few studies focus on the internal mechanism of this correlation or model this difference. Thus, in this paper, we proposed and applied a mechanism error model for the lake water area estimated through remote sensing images with different spatial resolution. The manuscript is arranged as follows. Firstly, the difference of lake water areas estimated by two kinds of remote sensing images with different spatial resolutions is analyzed, and a mechanism model for lake surface area estimation is established based on several areal ground features of basic shape. Secondly, areas of Ebinur Lake based on different spatial

resolution images are used to validate this model. Finally, we discuss the effectiveness and limitation of this model as well as its implications.

2. Principles and Modeling

Mixed pixels are prevalent on water-land boundary on remote sensing images, especially on the low spatial resolution images. In general, there is no mixed pixel in the center of the lake. When using two images of different spatial resolutions acquired on the same time to identify lake water information respectively, the two results are nearly the same in the center and different on the water-land boundary because of the mixed pixels. In other words, the difference between the lake areas estimated by different resolution satellite images is mainly caused by the mixed pixels on the lake edge. Taking the area extracted by the high resolution image as reference, the error of the area extracted by the low resolution image is mainly determined by these mixed pixels.

In the next section, several internal homogeneous areal ground features of basic shape are used to calculate the numeric relationship between areas extracted from different spatial resolution images.

2.1. Elliptical (or Circular) Areal Ground Feature

For elliptical areal ground feature, Figure 1 shows the results extracted by remote sensing images with different spatial resolutions. The small ellipse and big ellipse represent the result derived from low spatial resolution image and high spatial resolution image, respectively. Set the center of the ellipse as the origin, and the two axes as X-axis and Y-axis, a Cartesian coordinate system is established. The result from the low spatial resolution image can be expressed as:

$$\begin{cases} x = R_x \cos\theta \\ y = R_y \sin\theta \end{cases}, \quad 0 \le \theta < 2\pi , \tag{1}$$

where R_x and R_y are positive real number, and denote the long and short radius of the result derived from low resolution image; θ is a parameter. Accordingly, the result from the high spatial resolution image can be expressed as:

$$\begin{cases} x = (R_x + d)\cos\theta \\ y = (R_y + d)\sin\theta \end{cases}, \quad 0 \le \theta < 2\pi , \tag{2}$$

where d is the difference between the two radii of the two ellipses.

Note that Figure 1 is only a schematic view. In the actual situation, the estimated area from the high spatial resolution image may be larger than that from the low resolution image, or maybe not. Thus, d can be positive of negative.

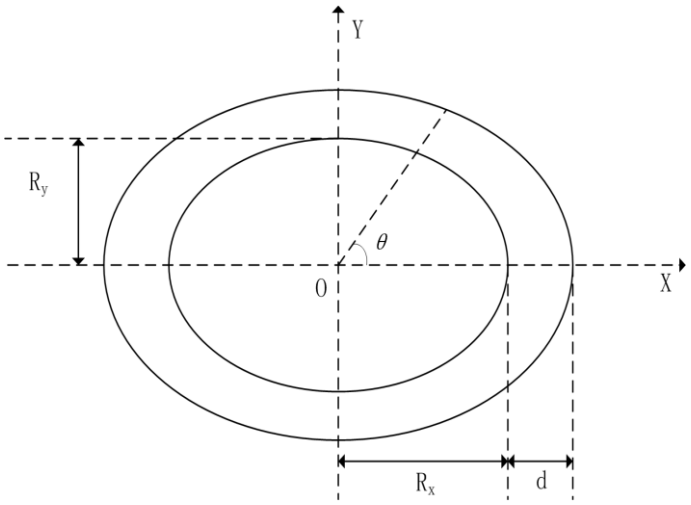

Figure 1. Extraction Results of Elliptical Areal Ground Feature based on the Different Spatial Resolution Images

S_h and S_l are used to represent the areas estimated from the high resolution image and low resolution image, respectively. According to the ellipse area formula, formula (3) is obtained:

$$\begin{aligned} S_h &= \pi (R_x + d)(R_y + d) = \pi R_x R_y + \pi d (R_x + R_y) + \pi d^2, \\ S_l &= \pi R_x R_y. \end{aligned} \tag{3}$$

Then, there is

$$S_h = S_l + \pi d (R_x + R_y) + \pi d^2.$$

If the ratio of R_x and R_y is fixed, set $R_y = mR_x$, then

$$\begin{aligned} S_l &= \pi m R_x^2, \\ R_x + R_y &= R_x + m R_x = (1 + m) R_x = \frac{1 + m}{\sqrt{\pi m}} \sqrt{S_l}. \end{aligned} \tag{4}$$

Set $k = \frac{1 + m}{\sqrt{\pi m}}$, then

$$R_x + R_y = k \sqrt{S_l}.$$

Hence

$$S_h = S_l + k \pi d \sqrt{S_l} + \pi d^2.$$

Let $a = -k \pi d$, $b = \pi d^2$, then there is

$$S_h = S_l - a \sqrt{S_l} + b, \tag{5}$$

where a and b are constants related to the geometry of the object and the difference between the spatial resolutions of the two images.

2.2. Triangle Areal Ground Feature

For triangle areal ground feature (Figure 2), triangle A'B'C' is the estimation from high resolution image and triangle ABC is that from low resolution image. Triangle ABC and A'B'C' is similar with parallel corresponding sides. It can be inferred that the areas of Triangle A'B'C' (S_h) and ABC (S_l) also satisfy formula (5).

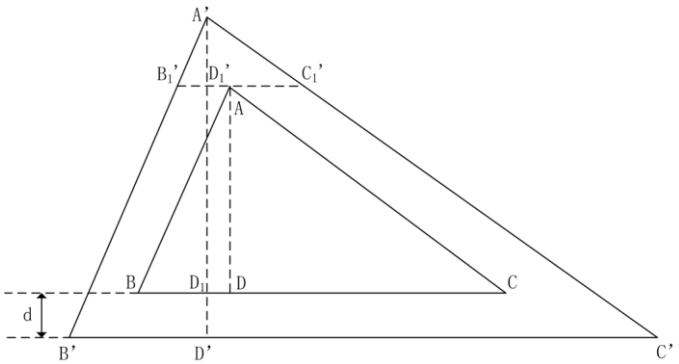

Figure 2. Extraction Results of Triangular Areal Ground Feature based on the Different Spatial Resolution Images

2.3. Areal Ground Feature with More General Shape

Since many of the common shapes can be decomposed into triangular, circular or oval, there are many features of other shapes satisfy formula (5). For example, the hexagonal feature in Figure 3. The inner hexagon is the estimation from the low resolution image and the outer one is that from the high resolution image. Obviously, S_h and S_l also satisfy formula (5).

For the above three areal ground features of different shapes, the estimations from high resolution image and low resolution satisfy formula (5). Parameters a and b differ with geometry of the object. It can be inferred that for internal homogeneous areal ground features, the estimations from different resolution satellite images cope with formula (5), of which the parameters are related to the geometry of the feature. Since the lake is an internal homogeneous feature to some extent, it should also cope with formula (5).Therefore, with a and b calculated based on the historical data, formula (5) could be a mechanism model and used to estimate the difference between lake water areas derived from low resolution image and high resolution image.

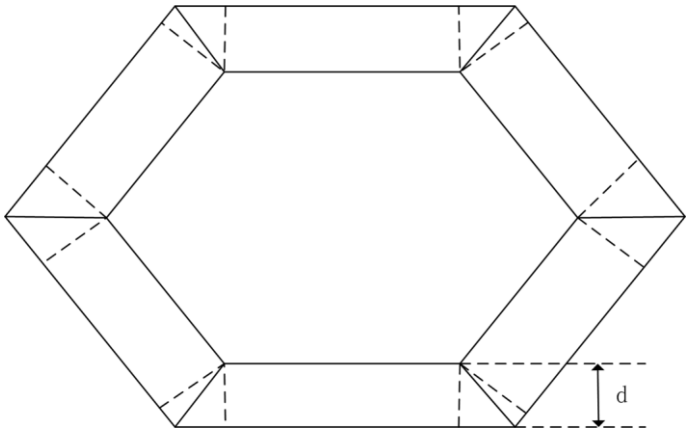

Figure 3. Extraction Results of Hexagonal Areal Ground Feature based on the Different Spatial Resolution Images

In general, compared with that from the low resolution image, the estimation from the high resolution image is closer to the true value. Thus, the mechanism model, formula (5), could be used to calibrate the estimated area from low resolution image as follows. Firstly, calculate a and b based on historical data. Then, calibrate the error of the estimation from low resolution image and obtain higher precision data. Note that the parameters are related to the geometry of the feature and the difference between the spatial resolutions of

the two images. Therefore, for some lakes with significant change in the geometry, the estimated areas could be divided into several segments according to S_l. In each segment, calculate the parameters and establish the model. This algorithm combines the advantages of the low resolution imagery and the high resolution imagery. That is, the temporal resolution of the result is consistent with the low spatial resolution imagery and the accuracy of the area is close to that from high spatial resolution imagery. This provides a new technique for the extraction of the lake area more accurately in a large area.

3. Model Validation

To validate the model, Ebinur Lake was selected as the study area. The lake surface areas derived with Moderate Resolution Imaging Spectroradiometer (MODIS), SPOT/VEGETATION (VGT) and Landsat Thematic Mapper (TM)/Enhanced Thematic Mapper (ETM) + were used.

3.1. Ebinur Lake Area Modeling Based On Landsat ETM+ and VGT Data

Ebinur Lake of Xinjiang province is a typical closed inland lake located in the arid region of north-western China, and it has an important impact on the local economic development and ecosystem. To obtain a continuous record of the change in lake area from 1998 to 2005, two indices, the Normalized Difference Vegetation Index (NDVI) and the Normalized Difference Water Index (NDWI), were selected to identify the water body based on the VGT data [14]. The ETM+ and China–Brazil Earth Resource Satellite (CBERS) CCD imagery with a higher spatial resolution was collected to validate the retrieved accuracy of the lake surface area from the VGT data. The ETM+ images at a resolution of 400m were downloaded from USGS Global Visualization Viewer (http://glovis.usgs.gov) website. Compared with the VGT imagery at a resolution of 1km, the ETM+ imagery is higher spatial resolution imagery. The comparison between the VGT estimate of the lake surface area and the ETM+ and CBERS CCD lake surface area was performed for the same periods in time. In this paper, we quote the lake surface areas derived with the VGT and ETM+ data. For ease of analysis, these data is divided into 16 sets according to the acquisition date of the imagery (Table 1).

Two ETM images acquired on September 25, 2001 and May 26, 2003 are shown in Figure 4, with lake surface area of 521 km^2 and 971 km^2, respectively.

According to the model, the difference between the lake surface areas estimated from high spatial resolution image and low spatial resolution image is a linear function of the square root of the area estimated from the low spatial resolution image, whereby the data in Table 1 was analyzed (Figure 5). It is shown that there is a linear relationship between the square root of the lake surface area derived with VGT and the difference between the lake surface areas derived with ETM and VGT, and this is a piecewise linear relationship with two segments. The last set of data at the first segment is (630, 714) and the first set of data at the second segment is (782, 721). With the lake surface area derived with VGT increased from 714 to 721, the linear relationship shows a dramatic change. In fact, although the relationship between the geometry of lake water surface and the area is continuous, the relationship changes very intensely in this interval. It is hardly to describe this variation exactly according to the existing data. Considering the practicality and economy of the model, here we no longer discuss the variation within the interval and just select 717.5 as a piecewise line. Set s as the square root of 717.5, which is approximately equal to 26.8.

Table 1. Ebinur Lake Surface Area (LSA) derived with Landsat ETM+ and VGT Data

Date	LSA derived with ETM+(km^2)	LSA derived with VGT(km^2)
1999.7.2	568	536
1999.8.3	551	591
1999.9.20	542	556
1999.11.7	555	685
2000.3.14	782	721
2000.6.18	804	722
2001.3.1	622	640
2001.7.7	580	517
2001.8.8	572	516
2001.11.12	630	714
2002.4.21	791	769
2002.5.23	885	801
2002.7.26	877	851
2002.9.28	808	784
2002.10.30	880	892
2003.5.26	971	994

Figure 4. Landsat ETM+ Images of Ebinur Lake

Whether the square root of the lake surface area derived with VGT is less than or greater than s, the relationship between the lake surface area derived with ETM+ and VGT is consistent with the model. It indicates that the model is consistent with the actual situation.

Figure 4 shows that a significant change occurs in the shape of Ebinur Lake surface on satellite imagery with the lake area increased. Thus, we infer the reason of the piecewise linear relationship in Figure 5 is as follows. The parameters of the model are related to the shape of the lake surface, and there is a significant change in the shape of the Ebinur Lake when the lake area is greater than a specific value. In this situation, the relationship between the lake surface area derived with ETM+ and VGT is still consistent with the model but the model parameters have a greater change.

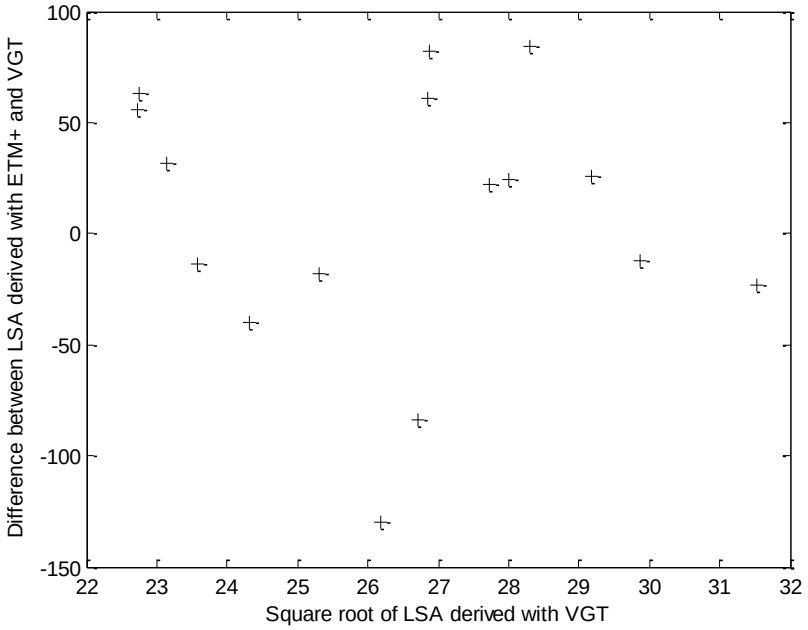

Figure 5. Relationship between Ebinur Lake Surface Area (LSA) Derived with Landsat ETM+ and VGT Data

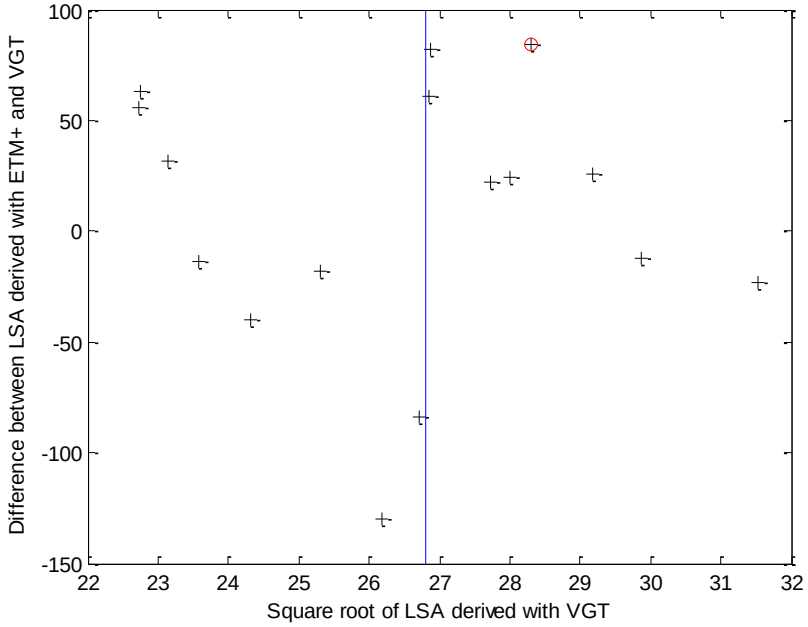

Figure 6. The PIECEWISE RELATIONSHIP between Ebinur Lake Surface Area (LSA) Derived with Landsat ETM+ and VGT Data

The data in Figure 5 are segmented with the vertical line so as to make it more intuitive (figure 6). S_h and S_l are used to represent the estimated area from ETM+ and VGT, respectively. The 16 sets of data (S_h, S_l) are sorted by S_l in ascending order, and it shows that a set of data (885, 801) is significantly different with the two adjacent sets of data (808, 784) and (877, 851). When S_l increased from 784 to 801, the corresponding S_h increased from 808 to 885, that is, S_h increased by 77. However, when S_l increased from 801 to 851, the corresponding S_h decreased from 885 to 877, that is, S_h decreased by 8. Therefore, we consider this set of data is not consistent with the overall trend of the data

and should be removed. As shown in Figure 6, the point in the circle is this set of data, and the vertical line is the piecewise line.

The remaining 15 sets of data were used to solve parameters of the piecewise model based on the least square method as follows. The collection of sample points can be expressed as:

$$\{(S_{h,i}, S_{l,i}) \mid i = 1, 2, \ldots k\}$$

where k=15. According to formula (5), the ideal value of the model parameters should satisfy the following formula:

$$\vec{S}_h - \vec{S}_l = P \begin{bmatrix} a \\ b \end{bmatrix},$$

where $\vec{S}_h = \begin{bmatrix} S_{h,1} & S_{h,2} & \ldots & S_{h,k} \end{bmatrix}^T$, $\vec{S}_l = \begin{bmatrix} S_{l,1} & S_{l,2} & \ldots & S_{l,k} \end{bmatrix}^T$, and $P = \begin{bmatrix} \sqrt{S_{l,1}} & 1 \\ \sqrt{S_{l,2}} & 1 \\ \ldots & \ldots \\ \sqrt{S_{l,k}} & 1 \end{bmatrix}$, which is the sample matrix. Then, the optimum values of the model parameters were calculated according to formula (6).

$$\begin{bmatrix} a \\ b \end{bmatrix} = (P^T P)^{-1} P^T (\vec{S}_h - \vec{S}_l). \quad (6)$$

Finally, the piecewise model was obtained:

$$S_c = S_l - 39.32\sqrt{S_l} + 940.20, \quad (7)$$

$$S_c = S_l - 19.53\sqrt{S_l} + 583.87, \quad (8)$$

where S_c is the calculated value of the model based on S_l. Figure 7 shows this model. For each value of S_l, the corresponding value of S_c was calculated according to formula (7) or (8) (Table 2). The 'No' refers to the sorting number mentioned previously, and the No.13 is the data removed.

Taking S_h as reference, it is shown that the minimum absolute value of error of S_l is 12, the maximum is 130, and the mean is 45.8. The minimum absolute value of the error percentage of S_l is 1.36%, the maximum is 23.42%, and the mean is 7.08%. For S_c, the minimum absolute value of the residual is 1.64, the maximum is 40.89, and the mean is 18.33. The minimum absolute value of the residual percentage is 0.21%, the maximum is 7.37%, and the mean is 2.85%. The comparison between the error and residual percentage shows that S_c is closer to S_h than S_l. The distribution of the error percentage and residual percentage indicates that the error of lake area extracted by VGT is unstable while the residual of S_c is more concentrated with smaller range. Overall, compared with the lake suface areas derived from VGT, the calculated values are closer to those derived from ETM+. Below an example will be used to show the prospect of this model: calibrating area extracted by low spatial resolution imagery to obtain more accurate data. In other words, if at a certain time, the accuracy of the area extracted by satellite imagery cannot meet the actual need, this area could be calibrated based on the error model and historical area data to improve the accuracy. This process is as follows. Firstly, remove the outliers of historical data. Secondly, calculate the model parameters based on the remaining historical data. Finally, calibrate the area extracted by low spatial resolution imagery based on the model.

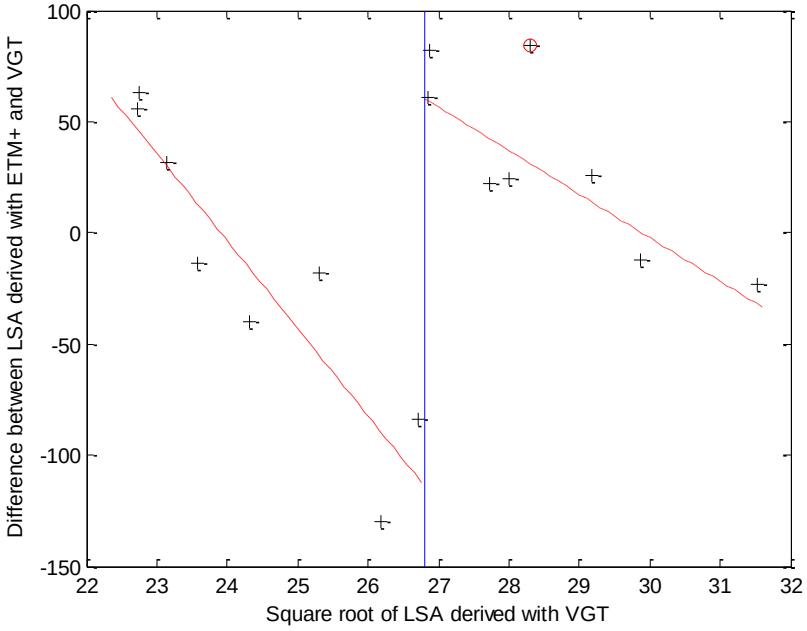

Figure 7. Parameters Solution

Table 2. Ebinur Lake Surface Area (LSA) Derived from VGT Data and from Calculation Results of the Model

No	LSA derived with ETM+ (km^2)	LSA derived with VGT (km^2)	Error of LSA derived with VGT(km^2)	Error percentage (%)	Calculation Value(km^2)	Residual (km^2)	Residual percentage (%)
1	572	516	-56	-9.79	562.84	-9.16	-1.60+**
2	580	517	-63	-10.86	562.98	-17.02	-2.93+
3	568	536	-32	-5.63	565.70	-2.30	-0.40+
4	542	556	14	2.58	568.86	26.86	4.96
5	551	591	40	7.26	575.12	24.12	4.38+
6	622	640	18	2.89	585.28	-36.72	-5.90
7	555	685	130	23.42	595.89	40.89	7.37+
8	630	714	84	13.33	603.33	-26.67	-4.23+
9	782	721	61	-7.80	780.36	-1.64	-0.21+
10	804	722	-82	-10.20	781.00	-23.00	-2.86+
11	791	769	-22	-2.78	811.19	20.19	2.55+
12	808	784	-24	-2.97	820.93	12.93	1.60+
14	877	851	-26	-2.96	865.04	-11.96	-1.36+
15	880	892	12	1.36	892.47	12.47	1.42
16	971	994	23	2.37	962.02	-8.98	-0.92+
Mean absolute value	\	\	45.8	7.08	\	18.33	2.85

** "+" means that the accuracy of calculation value is higher than the lake surface area derived with VGT

The lake surface area data (580, 517) on July 7, 2001 was employed to demonstrate the calibration process. Assuming that we lack the ETM+ imagery acquired on July 7, 2001, and try to calibrate the lake surface area derived from VGT imagery on the same day based on the error model. Since this set of data is at the first segment of the model, the parameters in formula (7) need to be recalculated. The calculation process is the same as the original argument, but the data (580, 517) is removed in the least square algorithm. Finally, formula (9) is obtained:

$$S_c = S_l - 37.14\sqrt{S_l} + 884.07 \tag{9}$$

Set S_l=517, then S_c=556. Before calibration, the difference percentage between the lake surface areas derived with VGT and ETM+ is -10.86%; after calibration, this value decreased to -4.138%. Obviously, the accuracy of the lake surface area derived with VGT data has improved significantly.

However, the comparison between formula (7) and (9) shows that the parameters are significantly different, especially the value of b changes more than 5%, indicating that existing sample data is not enough, even if only one sample reduction will have an impact on the results. Thus, the above calibration result is just the initial application of the error model when the number of samples is small, and there are potential for improving calibration accuracy. With the gradual accumulation of sample data, the model will tend to be stable and reflect the best calibration effect. In practice, sometimes the remote sensing images we collected cannot completely cover the entire monitoring period, that is, we lack images in certain period of time. In these periods, a possible solution is to use imagery with lower spatial resolution but higher temporal resolution. Then the mechanism model proposed in this paper could be used to improve the accuracy of the area derived with low spatial resolution imagery. The process is as follows. Firstly, collect low spatial resolution images acquired on the same time with existing high spatial resolution images as more as possible, and estimate the lake surface area by the low spatial resolution images. Secondly, establish the model based on the area data derived with the two kinds of images of the same periods in time. Finally, for the period lacks of high spatial resolution imagery, extract the lake surface area by low spatial resolution imagery, then use the model to calibrate it.

3.2. Calibration of Ebinur Lake Area from MODIS Data with Landsat TM/ETM+ Data

The theory of the model and its calibration effect of the VGT imagery are validated above based on the Ebinur Lake surface areas derived with the VGT and Landsat ETM+ data. In this section, the Ebinur Lake surface areas derived with Landsat TM/ETM+ data and MODIS data are used to further validate the calibration capacity of the model for low spatial resolution data. Landsat TM/ETM+ images at a resolution of 30 m were downloaded from USGS Global Visualization Viewer (http://glovis.usgs.gov) website, and the MODIS images at a resolution of 500 m were downloaded from USGS ftp site (ftp:// e4ftl01.cr.usgs.gov). To ensure the comparability of the lake surface areas from MODIS and TM/ETM+ data, the water information identification based on the same method, and the corresponding images nearly acquired on the same day (table 3). S_h and S_l are used to represent the lake surface areas derived from Landsat TM/ETM+ and MODIS, respectively.

The NDWI is designed to enhance water features and suppress vegetation and soil, and it is expressed as follows [18]:

$$NDWI = \frac{Green - NIR}{Green + NIR}, \tag{10}$$

where Green is the reflectance of a green band such as TM band 2, and NIR is the reflectance of a near-infrared band such as TM band 4. However, the extracted water information in the regions with a built-up land background was often mixed with built-up land noise [19]. Considering that the reflectance of water body in the near-infrared band is much smaller that of soil and built-up land, a combined model of NDWI and near-infrared (NIR) is selected for the identification of water bodies in Ebinur Lake. This model can be expressed as:

$$NDWI > A \,\&\, NIR < B\,, \tag{11}$$

where A and B are thresholds. To improve the accuracy of extracted water information, for each Landsat TM/ETM+ and MODIS image the Iterative method was used to determine the thresholds independently[20].

Table3. Ebinur Lake Surface Area (LSA) Derived from Landsat TM/ETM+ and MODIS Data

Date	LSA derived with TM/ETM+ (km^2)	LSA derived with MODIS (km^2)
2002.5.23	851.00	840.75
2003.5.26	970.16	967.50
2006.8.22	506.79	493.75
2008.7.2	544.02	557.25
2008.8.3	445.05	471.00
2009.6.19	465.77	479.50
2009.7.21	424.18	432.00
2011.7.11	552.23	583.25

The lake surface area (544.02，557.25) on July 2, 2008 was employed to validate the calibration capacity of this model for estimated lake area from low spatial resolution imagery. Although the number of samples is small than that in 3.1, the remaining data still shows that there is a linear relationship between the square root of the lake surface area derived with MODIS and the difference between the lake surface areas derived with TM/ETM+ and MODIS, and this is also a piecewise linear relationship (figure 8). In addition, the piecewise line is basically the same as that in figure 6. It indicates that the relationship between the lake surface areas derived from TM/ETM+ and MODIS data is also consistent with the model, and the lake area derived from MODIS can be calibrated based on this model.

The validation process is as follows. Firstly, calculate the model parameters based on the remaining data. Secondly, calibrate the lake surface area derived from MODIS (557.25) using the model. Finally, compare the calibrated area with that derived from TM/ETM+ (544.02). Since the area data (544.02, 557.25) is at the first segment of the model, the 5 sets of data at this segment was used to calculate the model parameters based on the least square method (figure 9), and formula (12) is obtained:

$$S_c = S_l - 5.75\sqrt{S_l} + 114.35\,. \tag{12}$$

Set S_l=557.25, then S_c=535.78. Before calibration, the difference percentage between the lake surface areas derived with MODIS and TM/ETM+ is 2.43%; after calibration, this value decreased to -1.51%. It shows that the accuracy of the lake surface area derived with MODIS data has improved to some extent.

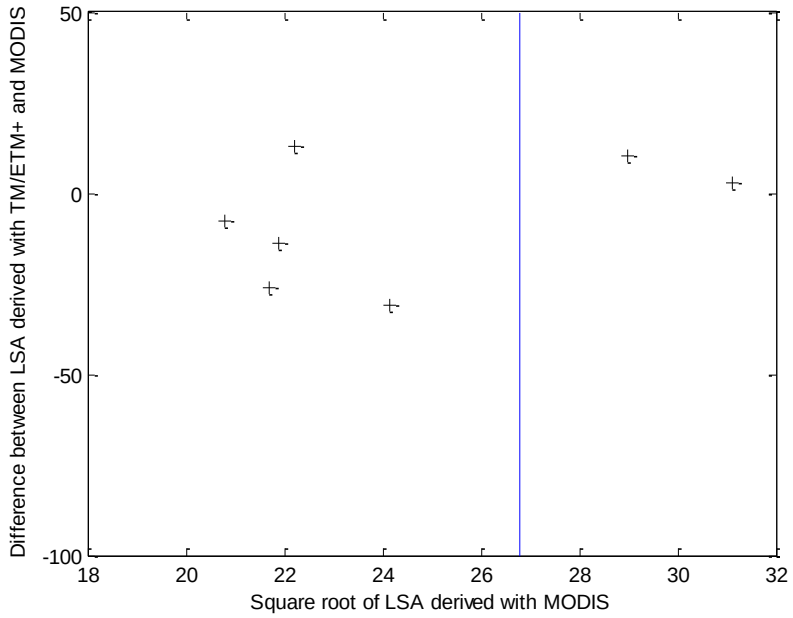

Figure 8. Relationship between Ebinur Lake Surface Areas Derived with Landsat TM/ETM+ and MODIS Data

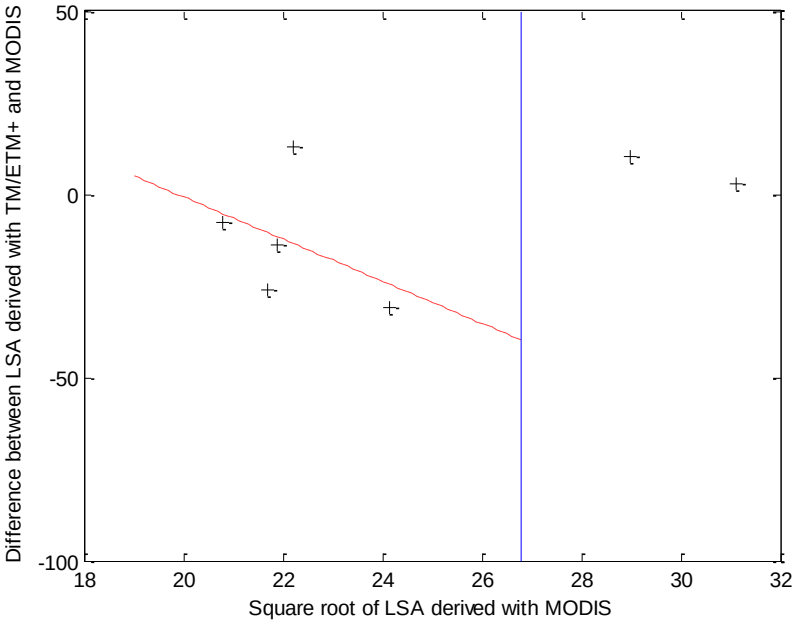

Figure 9. Parameters Solution

4. Conclusions and Discussion

The difference between the lake water surfaces derived with different spatial resolution satellite images is mainly caused by the mixed pixels on the water-land boundary rather than the pixels inside the lake. Previous studies showed that the lake surface area values derived from different spatial resolution images are strongly correlated, yet the numerical relationship between the two areas was rarely studied. In general, the shape of lake water surface is irregular, thus it is difficult to derive the relationship directly. For this reason, the elliptical (including circular), triangular and hexagonal areal features are selected to deduce the relationship between the areas derived from different spatial resolution

images, which is used to infer the numerical relationship between the lake surface areas derived with different resolution images. This relationship can be used as a mechanism model for the difference between the lake surface areas estimated through remote sensing images with different spatial resolution. Taking the area derived from high resolution image as reference, this model can be used to estimate the error of the area derived from low resolution image to a certain extent. The application in Ebinur Lake validates the principle of the model, indicating that the model is consistent with the actual situation. In addition, this model can be used to calibrate the lake surface area derived from low spatial resolution imagery with high resolution imagery. Taking the lake surface area extracted by ETM+ as reference, the error percentage of the area extracted by VGT decreased from -10.86% to -4.138% after calibration based on this model. This result validates the high resolution imagery can be used to calibrate the area estimated by low resolution imagery and also shows that the model proposed in this paper has the ability to calibrate the lake surface area extracted from low resolution imagery. The calibration of Ebinur Lake water area from MODIS data assisted with Land TM/ETM+ data further validate this application prospect.

In this paper, the effectiveness and applicability of the model is validated based on the Ebinur Lake. Consider that the model parameters are closely related to the shape of the lake surface, we will apply this model to other lakes in the future, on this basis a further analysis on the relationship between the parameters and the shape of the lake water surface can be performed. In addition, this model is not based on satellite imagery with a specific spatial resolution, thus, it can apply to any two images with different spatial resolution, for example, MODIS and SPOT, or QuickBird and TM at a higher spatial resolution.

Acknowledgments

This research was supported by the Scientific and Technological Research Program of Chongqing Municipal Education Commission (Grant No.KJ131108).

References

[1] Y. J. Ding, S. Y. Liu, B. S. Ye and L. Zhao, "Climatic implications on variations of lakes in the cold and arid regions of China during the recent 50 years", Journal of Glaciology and Geocryology, vol. 28, no. 5, **(2006)**, pp. 623-632.
[2] Z. G. Hu, Y. T. Wang, T. H. Chi, S. H. Liu and J. T. Bi, "Monitoring lake areas based on mixed pixel decomposition combined with double-edge extraction", Remote Sensing Information, no. 3, **(2007)**, pp. 34-38.
[3] B. S. Zhu, S. H. Zhang, D. L. Xu and W. C. Meng, "Comprehensive water index and its application", Journal of Geomatics Science and Technology, vol. 30, no. 1, **(2013)**, pp. 19-23.
[4] F. M. Hui, B. Xu, H. B. Huang, Y. Qian and P. Gong, "Modeling spatial-temporal change of Poyang Lake using multitemporal Landsat imagery", International Journal of Remote Sensing, vol. 29, no. 20, **(2008)**, pp. 5767-5784.
[5] J. Wang, S. L. Lu, B. F. Wu, N. N. Yan and L. Pei, "Land cover change in Baiyangdian wetland", Journal of Geo-information Science, vol. 12, no. 2, **(2010)**, pp. 292-300.
[6] R. X. Liu and Y. J. Liu, "Area changes of Lake Qinghai in the latest 20 years based on remote sensing study", Journal of Lake Sciences, vol. 20, no. 1, **(2008)**, pp. 135-138.
[7] L. Feng, C. M. Hu, X. L. Chen, X. B. Cai, L. Q. Tian and W. X. Gan, "Assessment of inundation changes of Poyang Lake using MODIS observations between 2000 and 2010", Remote Sensing of Environment, no. 121, **(2012)**, pp. 80-92.
[8] C. Z. Liu, J. C. Shi, S. Gao and L. Chen, "The study on extracting of water body from MODIS image using an improved linear mixture model", Remote Sensing Information, no. 1, **(2010)**, pp. 84-88.
[9] H. E. Zhang, J. C. Shi and S. H. Liu, "Sub-pixel lakes mapping in Tibetan Plateau", Advances in Water Science, vol. 17, no. 3, **(2006)**, pp. 376-382.
[10] C. Yuan and X. W. Zhao, "Calibration of NOAA satellite data with Landsat TM data", Journal of Remote Sensing, vol. 4, no. 4, **(2000)**, pp. 266-270.
[11] S. Li, W. Z. Li, J. J. Zhou and D. F. Zhuang, "A review on endmember selection methods in the course of mixed pixel decomposition of remote sensing images", Geography and Geo-Information Science, vol. 23, no. 5, **(2007)**, pp. 35-42.

[12] H. L. Fang, B. F. Wu, H. Y. Liu and X. Huang, "Using NOAA AVHRR and Landsat TM to estimate rice area year-by-year", International Journal of Remote Sensing, vol. 19, no. 3, **(1998)**, pp. 521-525.
[13] J. F. Gao, X. S. Jiang, S. G. Liu and J. J. Pan, "Monitoring of paddy plantation area on the county-level with ETM-assisted MODIS. Soils", vol. 40, no. 3, **(2008)**, pp. 484-489.
[14] X. Zheng and J. J. Zhu, "Estimation of shelter forest area in Three-North Shelter Forest Program region based on multi-sensor remote sensing data", Chinese Journal of Applied Ecology, vol. 24, no. 8, **(2013)**, pp. 2257-2264.
[15] X. D. Li, Y. Du and F. Ling, "Super-Resolution Mapping of Forests With Bitemporal Different Spatial Resolution Images Based on the Spatial-Temporal Markov Random Field", IEEE Journal of Selected Topics in Applied Earth Observation and Remote Sensing, vol. 7, no. 1, **(2013)**, pp. 29-39.
[16] P. Kempeneers, F. Sedano, L. M. Seebach, P. Strobl and J. San-Miguel-Ayanz, "Data Fusion of Different Spatial Resolution Remote Sensing Images Applied to Forest-Type Mapping", IEEE Transactions on Geoscience and Remote Sensing, vol. 49, no. 12, **(2011)**, pp. 4977-4986.
[17] M. G. Ma, X. Wang, F. Veroustraete and L. Dong, "Change in area of Ebinur Lake during the 1998-2005 period", International Journal of Remote Sensing, vol. 28, no. 24, **(2007)**, pp. 5523-5533.
[18] S. K. Mcfeeters, "The use of normalized difference water index (NDWI) in the delineation of open water features", International Journal of Remote Sensing, vol. 17, no. 7, **(1996)**, pp. 1425-1432.
[19] H. Q. Xu, "Modification of normalized difference water index (NDWI) to enhance open water features in remotely sensed imagery", International Journal of Remote Sensing, vol. 27, no. 14, **(2006)**, pp. 3025-3033.
[20] N. N. Chen, "Achieve and comparison of image segmentation thresholding method", Computer Knowledge and Technology, vol. 7, no. 13, **(2011)**, pp. 3109-3111.

Author

Rong Xu, she received her PhD in cartography and geographic information system (1991) from University of Chinese Academy of Sciences. Now she works at the School of Computer Science and Engineering, Chongqing Three Gorges University. She is making research on the information science and technology.

